J Therm Anal Calorim (2010) 99:357–362
DOI 10.1007/s10973-009-0096-2

Non-isothermal decomposition kinetics of synthetic serrabrancaite ($MnPO_4 \cdot H_2O$) precursor in N_2 atmosphere

Banjong Boonchom · Chanaiporn Danvirutai · Montree Thongkam

Received: 20 December 2008 / Accepted: 11 February 2009 / Published online: 23 June 2009

Abstract The thermal decomposition of synthetic serrabrancaite ($MnPO_4 \cdot H_2O$) was studied in N_2 atmosphere using TG-DTG-DTA. Thermal analysis results indicate that the decomposition occurs in two stages, which are assigned to the dehydration and the reduction processes and the final product is $Mn_2P_2O_7$. X-ray powder diffraction, FT-IR and FT-Raman techniques were used for identification of the solid decomposition product. The decomposition kinetics analysis of $MnPO_4 \cdot H_2O$ was performed under non-isothermal condition through isoconversional methods of Flynn–Wall–Ozawa (FWO) and Kissinger–Akahira–Sunose (KAS). The dependences of activation energies on the extent of conversions are observed in the dehydration and the reduction reactions, which could be concluded the "multi-step" processes.

Keywords Serrabrancaite · $MnPO_4 \cdot H_2O$ · Non-isothermal kinetics · Thermogravimetry

B. Boonchom (✉)
King Mongkut's Institute of Technology Ladkrabang, Chumphon Campus, 17/1 M. 6 Pha Thiew District, Chumphon 86160, Thailand
e-mail: kbbanjon@kmitl.ac.th

C. Danvirutai
Department of Chemistry, Faculty of Science, Khon Kaen University, Khon Kaen 40002, Thailand

M. Thongkam
Department of Chemistry, Faculty of Science, King Mongkut's Institute of Technology Ladkrabang, Ladkrabang, Bangkok 10520, Thailand

Introduction

Manganese phosphates are of considerable industrial interesting properties nowadays because of their wide applications in laser host [1], ceramic [2], dielectric [3], electric [4], magnetic [5], and catalytic [6] processes. Additionally, manganese phosphates are among the widest spread minerals in the class of phosphates [7, 8] such as MnP_3O_9 [9], $MnPO_4 \cdot H_2O$ [10] $MnPO_4$ [11], $MnHP_2O_7$ [12] and $Mn(PO_3)_3$ [13], MnP_4O_{11} [14], $Mn_2P_2O_7$ [15], β-$Mn_3(PO_4)_2$ [16] and $Mn_2P_2O_7 \cdot 2H_2O$ [17], etc.

$Mn_2P_2O_7$ has been found to have a wide range of applications such as catalyst and battery cell [6, 7, 15, 17]. In this respect, in the part few years many works have been undertaken a series of research studies on different preparative methods such as the thermal decomposition of $Mn_2P_2O_7 \cdot 2H_2O$, $Mn(H_2PO_2)_2 \cdot 2H_2O$ and $MnHPO_4 \cdot 3H_2O$ precursors [7, 17]. As part of this effort, we are currently undertaking a detailed thermal decomposition kinetics of $MnPO_4 \cdot H_2O$, which undergoes dehydration and reduction reactions [18–20]. This material provides synthetic challenges, as Mn^{3+} is prone to oxidation or reduction when heated or in aqueous solution. In many methods of kinetics estimation, isoconversional method is recommended as trustworthy way of obtaining reliable and consistent kinetic information [21, 22]. It is a 'model-free method', which involves measuring the temperatures corresponding to fixed values of the extent of conversion (α) from experiments at different heating rates (β). In the present study, the formation of $Mn_2P_2O_7$ from $MnPO_4 \cdot H_2O$ was followed using differential thermal analysis-thermogravimetry (TG-DTG-DTA), X-ray powder diffraction (XRD), Fourier transform-infrared (FT-IR) and Fourier transform-Raman (FT-Raman) techniques. The kinetics analysis of the non-isothermal results for dehydration and reduction steps of $MnPO_4 \cdot H_2O$

in was carried out using the isoconversional methods of Flynn–Wall–Ozawa (FWO) [23] and Kissinger–Akahira–Sunose (KAS) [24] and was reported for the first time.

Experimental procedures

Synthetic Serrabancaite, $MnPO_4 \cdot H_2O$ compound was prepared by solution precipitation method and characterized as previously described by the same authors [25]. Thermal analysis measurements (thermogravimetry, TG; differential thermogravimetry, DTG; and differential thermal analysis, DTA) were carried out by a Pyris Diamond Perkin Elmer apparatus by increasing temperature from 373 to 1,073 K with calcined α-Al_2O_3 powder as the standard reference. The experiments were performed in dynamic air at heating rates of 5, 10, 15, and 20 K min^{-1}. The sample mass was kept of about 8.0 ± 0.3 mg in an alumina pan without pressing. In accordance with thermal analysis results, the synthesized sample was thermally heated in a furnace until the completely dehydrated $Mn_2P_2O_7$ (pale pink) was obtained. The X-ray powder diffraction patterns of the prepared product and the calcined sample were obtained with a Bruker D8-Advanced model X-ray powder diffractometer with Cu Kα radiation ($\lambda = 0.15406$ Å). The room temperature FTIR spectrum of $Mn_2P_2O_7$ was recorded in the range of 4,000–370 cm^{-1} with eight scans on a Perkin-Elmer Spectrum GX FT-IR/FT-Raman spectrometer with the resolution of 4 cm^{-1} using KBr pellets (KBr, Jasco, spectroscopy grade). The FT-Raman spectrum of $Mn_2P_2O_7$ was recorded with spectrum 2000R NIR FT-Raman system in a Perkin-Elmer Spectrum GX model equipped with a HeNe laser (1,064 nm). The laser power about 500 mW was used for excitation in the range between 4,000 and 100 cm^{-1} with 32 scans.

Result and discussion

The TG curves of $MnPO_4 \cdot H_2O$ at four heating rates (5, 10, 15, and 20 K min^{-1}) are shown in Fig. 1a. All curves are approximately in the same shape and indicated that the mass loss is independent of the heating rate. All curves showed that two thermal decomposition steps of $MnPO_4 \cdot H_2O$ below 873 K All peaks in the DTG and DTA curves (Fig. 1b) closely correspond to the mass loss observed on the TG traces. Additionally, two decomposition stages were shifted toward higher temperatures when the heating rates increase. The mass loss of the first step (at about 482–617 K) at all four heating rates is between 2.43 and 2.56%, which is close to the mass loss of the release of 0.2–0.3 water molecules [26]. This can be ascribed to the

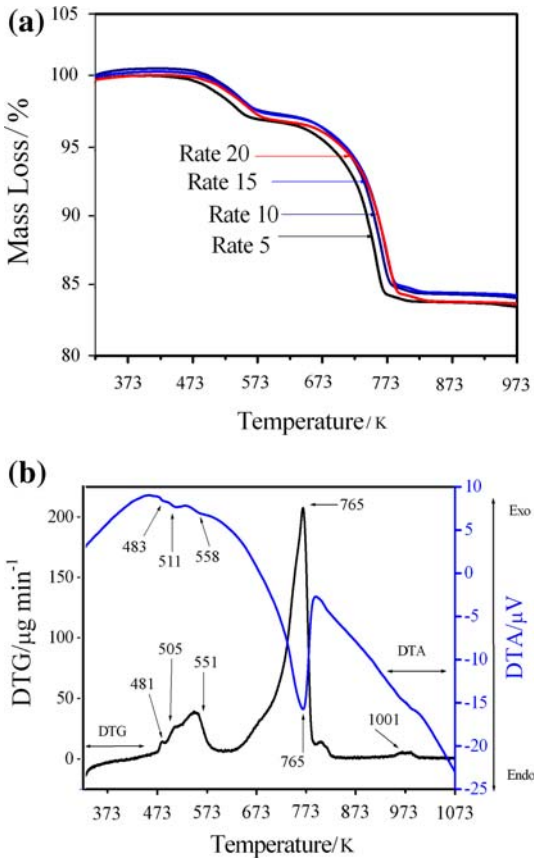

Fig. 1 TG curves of $MnPO_4 \cdot H_2O$ in N_2 atmosphere at four heating rates (5, 10, 15 and 20 K min^{-1}) (**a**); DTG-DTA curves of $MnPO_4 \cdot H_2O$ in N_2 atmosphere at heating rate 10 K min^{-1} (**b**)

dehydration of $MnPO_4 \cdot H_2O$ due to the water of crystallization.

The second mass loss step of $MnPO_4 \cdot H_2O$ relates with the consequent release of oxygen and a water molecule, which is referred the reduction reaction (Mn(III) to Mn(II)) [19, 20]. The mass loss of this step (at about 618–833 K) is about 13.02%, which contains 5.15% of O_2 and 7.87% of H_2O. The mass loss is accompanied by a change of colour from gray–green to pale pink. The DTG and DTA curves at heating rates of 10 K min^{-1} are shown five peaks at about 481, 505, 551, 765, and 1,001 K and four endothermic effects at about 483, 511, 558, and 765 K, respectively. The synthetic $MnPO_4 \cdot H_2O$ is a very similar mass loss and transformation reaction, which are also described by Lightfoot et al. [10]. The overall reaction involves the dehydration and reduction processes as shown in Eqs. 1 and 2:

$$MnPO_4 \cdot nH_2O \rightarrow MnPO_4 \cdot (n - 0.3)H_2O + \sim 0.3H_2O \quad (1)$$

$$MnPO_4 \cdot (n - 0.3)H_2O \rightarrow 0.5Mn_2P_2O_7 + 0.5\ O_2 + \sim 1H_2O \quad (2)$$

$(1 < n < 1.3)$

The XRD patterns of synthetic $MnPO_4 \cdot nH_2O$ and its decomposition product ($Mn_2P_2O_7$) are shown in Fig. 2. The standard XRD patterns of $MnPO_4 \cdot H_2O$ (PDF #440071) and $Mn_2P_2O_7$ (PDF#771243) indicate that both crystal structures are monoclinic system with space group C2/c ($Z = 4$) and C2/m ($Z = 2$), respectively. The XRD data has been reported in our previously work [25].

The formation of nanocrystalline $Mn_2P_2O_7$ sample is further supported by FTIR and FT-Raman spectra in the range of 4,000–370 amd 4,000–100 cm^{-1}, respectively (Fig. 3 a, b). The FTIR and FT-Raman bands are identified in term of the fundamental vibrating units namely $P_2O_7^{4-}$ anion, which is very similar to this observed in the literatures [27–29]. The observed bands at 3,424 and 1,633 cm^{-1} of the FTIR spectra are assigned to the asymmetric stretching (v_3) and bending mode (v_2) of absorbed moisture of KBr pellet. The P–O stretching modes of the $[P_2O_7]^{4+}$ anion are known to appear in the 1,250–975 cm^{-1} region [27, 28]. The symmetric PO_2 stretching vibrations (v_{sym} PO_2) for the $Mn_2P_2O_7$ sample are observed in the rage of 1,000–1,100 cm^{-1}, while the asymmetric stretching vibrations (v_{asym} PO_2) are located at 1,100 and 1,200 cm^{-1}. The asymmetric (v_{asym} POP) and symmetric stretch (v_{sym} POP) bridge vibrations for this samples are observed in 900–1,000 and 400–700 cm^{-1}, respectively. The PO_3 deformation, rocking modes, the POP deformations, the torsional and external modes are found in the 400–230 cm^{-1} region [29].

Decomposition of crystal hydrates is a solid-state process of the type [30]: A (solid) → B (solid) + C (gas). The kinetics of such reactions is described by various equations taking into account the special features of their mechanisms. This is a model-free method, which involves measuring the temperatures corresponding to fixed values of α from experiments at different heating rates (β). The

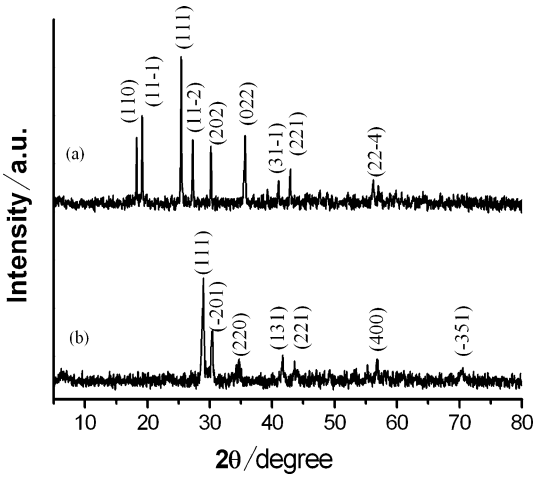

Fig. 2 The XRD patterns of serrabrancaite $MnPO_4 \cdot H_2O$ (**a**) and its dehydration product ($Mn_2P_2O_7$) (**b**)

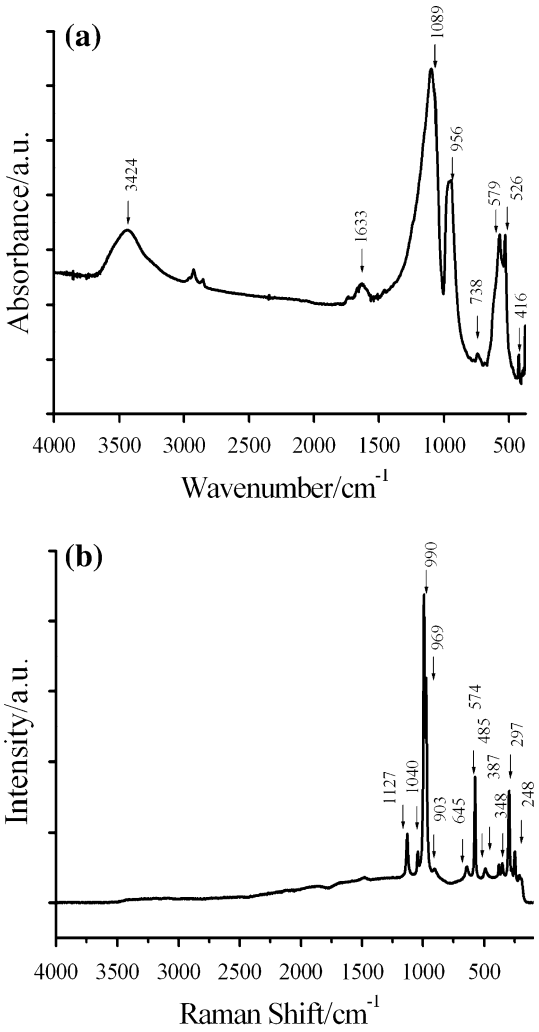

Fig. 3 FT-IR (in the range of 4,000–370 cm^{-1}) (**a**) and FT-Raman (in the range of 4,000–100 cm^{-1}) (**b**) spectra of $Mn_2P_2O_7$

activation energies (E_α) can be calculated according to the isoconventional methods. In kinetic study of $MnPO_4 \cdot H_2O$, FWO [23] and KAS [24] equations were used to determine the activation energy of the dehydration reaction.

The equations used for E_α calculation are:

Flynn–Wall–Ozawa equation:

$$\ln \beta = \ln\left(\frac{AE_\alpha}{R\,g(\alpha)}\right) - 5.3305 - 1.0516\left(\frac{E_\alpha}{RT}\right) \quad (3)$$

KAS equation:

$$\ln\left(\frac{\beta}{T^2}\right) = \ln\left(\frac{AE_\alpha}{R\,g(\alpha)}\right) - \left(\frac{E_\alpha}{RT}\right) \quad (4)$$

where A (the pre-exponential factor) and E (the activation energy) are the Arrhenius parameters and R is the gas constant (8.314 J mol^{-1} K^{-1}). The Arrhenius parameters, together with the reaction model, are sometimes called the

kinetic triplet. $g(\alpha) = \int_0^{\alpha} \frac{d\alpha}{f(\alpha)}$ is the integral form of $f(\alpha)$, which is the reaction model that depends on the reaction mechanism.

At the constant condition of others parameters, the TG curves for dehydration and reduction process of $MnPO_4 \cdot H_2O$ in N_2 atmosphere at various heating rates (5, 10, 15 and 20 °C min^{-1}) are shown in Fig. 1a. According to isoconversional method, the basic data of α and T collected from Fig. 1a are illustrated in Tables 1 and 2, respectively. According to the above-mentioned equations, the plots of ln β versus 1,000 T^{-1} (FWO) and ln β/T^{-2} versus 1,000 T^{-1} (KAS) corresponding to different conversions α can be obtained by a linear regression of least-square method. The activation energies E_α can be calculated from the slopes of straight lines with better linear correlation coefficient (r^2). The slopes change depending on the degree of conversion (α) for the dehydration and reduction reaction of $MnPO_4 \cdot H_2O$. The α-dependences of the apparent E_α values for the dehydration and reduction reactions of $MnPO_4 \cdot H_2O$ calculated from the slopes of Eqs. 3 and 4 at various α are shown in Tables 3 and 4, respectively. If E_α varies with α, the results should be interpreted in terms of multi-step reaction mechanism [21, 22, 30–36]. Unfortunately there is rather all the information available. Considering different conversion functions $f(\alpha)$, a series of values for the pre-exponential factor should be obtained, but this is rather a mathematical exercise but not a kinetic analysis [31–33].

The activation energy values of dehydration process of $MnPO_4 \cdot H_2O$ were found between 217.53 and 844.12 kJ mol^{-1} by using FWO and KAS methods, which are also higher than those of the dehydration reactions of some phosphate hydrates ($FePO_4 \cdot H_2O$, $AlPO_4 \cdot H_2O$ and $Mn(H_2PO_4)_2 \cdot 2H_2O$). The activation energy values increase largely in the increasing α (0.2–0.8) (Table 3), so we draw a conclusion that the dehydration of $MnPO_4 \cdot H_2O$ may be a multi-step reaction, which is different from the single step in some metal phosphates above [22, 37–41].

The activation energy values of reduction step were calculated between 1919.67 and 5687.03 kJ mol^{-1} by using FWO method and close to the calculated by the KAS method but higher than the other reactions [30–33]. It is clear in Table 4, that the activation energy assumes a value of 1919.67 kJ mol^{-1} at the beginning of the decomposition reaction and, with increasing mass loss, ups to a value of 5418.94 kJ mol^{-1} (FWO) method). This increasing

Table 1 The $\alpha - T$ data at different heating rates, β (K min^{-1}) for the dehydration step of $MnPO_4 \cdot H_2O$ (453.15–523.15 K)

α	Temperature/K			
	$\beta = 5$	$\beta = 10$	$\beta = 15$	$\beta = 20$
0.2	485.91	492.79	495.92	497.93
0.3	490.47	497.18	500.27	502.58
0.4	494.90	500.95	503.93	505.97
0.5	499.34	504.42	507.44	509.21
0.6	504.20	507.92	510.50	512.02
0.7	509.29	511.64	513.62	515.01
0.8	514.29	515.49	516.94	517.77

Table 2 The α and T data at different heating rates, β (K min^{-1}) for the reduction step of $MnPO_4 \cdot H_2O$ (673.15–873.15 K)

α	Temperature/K			
	$\beta = 5$	$\beta = 10$	$\beta = 15$	$\beta = 20$
0.2	646.02	647.07	647.13	647.47
0.3	654.78	656.22	656.62	657.28
0.4	661.66	663.12	663.89	664.52
0.5	667.52	668.75	669.38	670.18
0.6	672.69	673.67	674.40	675.12
0.7	677.41	678.27	678.79	679.38
0.8	681.73	682.32	682.78	683.24

Table 3 Activation energies E_α and correlation coefficient (r^2) calculated by FWO and KAS methods for the dehydration step of $MnPO_4 \cdot H_2O$ (453.15–523.15 K)

α	FWO method		KAS method	
	E_α/kJ mol^{-1}	r^2	E_α/kJ mol^{-1}	r^2
0.2	217.53	0.9926	220.57	0.9921
0.3	221.99	0.9957	225.19	0.9954
0.4	246.31	0.9967	250.71	0.9965
0.5	279.44	0.9989	285.47	0.9988
0.6	358.48	0.9990	368.54	0.9989
0.7	499.13	0.9912	516.37	0.9909
0.8	810.90	0.9727	844.12	0.9722

Table 4 Activation energies E_α and correlation coefficient (r^2) calculated by FWO and KAS methods for the reduction step of $MnPO_4 \cdot H_2O$ (673.15–873.15 K)

α	FWO method		KAS method	
	E_α/kJ mol^{-1}	r^2	E_α/kJ mol^{-1}	r^2
0.2	1919.67	0.9844	2007.83	0.9843
0.3	1694.26	0.9996	1770.63	0.9996
0.4	1882.16	0.9901	1968.09	0.9900
0.5	2059.11	0.9854	2154.16	0.9853
0.6	2597.06	0.9886	2719.84	0.9885
0.7	3402.24	0.9811	3566.37	0.9810
0.8	5418.94	0.9502	5687.03	0.9500

dependence of E_α on α indicates that the overall reaction contains a least two steps, and the kinetics scheme of which corresponds top a reversible reaction followed by an irreversible one [33–35]. The larger activation energy at the beginning of the reaction may be due to the additional destruction of crystal structure, which is related to reduction of Mn^{3+} to Mn^{2+} and then the consequent release of oxygen while the smaller activation energy at the end of the reaction due to the weight loss of about one water molecule[18]. The reduction step (2nd) exhibits higher activation energy in comparison with the dehydration step (1st), and this is understandable because this step corresponds to a reduction of Mn^{3+} to Mn^{2}, in connection with polycondensation reaction [10, 18–20]. This result confirmed that the decomposition product ($Mn_2P_2O_7$) was obtained. The activation energies calculated in N_2 atmosphere for two decomposition of $MnPO_4 \cdot H_2O$ is higher than those reported previously for the decomposition of $MnHPO_4 \cdot H_2O$, $FePO_4 \cdot 3H_2O$, $Mn(H_2PO_4)_2 \cdot 2H_2O$ under air atmosphere [37–41]. However, the activation energies of the two decomposition reactions of the studied compound are close to those observed in the decomposition of $Mn(H_2PO_2)_2 \cdot 2H_2O$ [42] under N_2 atmosphere. The activation energies and the multi-step processes of two reactions for the studied compound may be its characteristic; the strong effect of water of crystallization within this structure and metal reduction process before polycondensation reaction. Additionally, these results indicate that the atmosphere for thermal transformation of $MnPO_4 \cdot H_2O$ have the strong effect on the activation energies. In this respect, these data will be important for further studies of the studied compounds, which include studies under carefully controlled reaction conditions.

Conclusion

The synthetic serrabrancaite ($MnPO_4 \cdot H_2O$) decomposes in two steps, which undergoes dehydration and reduction reactions. The dehydration is the elimination of a little amount water, while the reduction step is due to the reduction of Mn^{3+} to Mn^{2+} and the consequent release of oxygen and water molecules, respectively. For the dehydration and reduction reactions of synthetic $MnPO_4 \cdot H_2O$, the activation energy values calculated by using FWO method are close to those by KAS method, and the respective correlation coefficients are preference, which were reported for the first time. On the basis of correctly established values of the apparent activation energy, certain conclusions can be made concerning the mechanisms and characteristics of the processes. The data of kinetics play an important role in theoretical study, application development and industrial production of a compound as a basis of theoretical. Additionally, various scientific and practical problems involving the participation of solid phases can be solved.

Acknowledgments The authors would like to thank the Chemistry Department, Khon Kaen University for providing research facilities. This work is financially supported by the Thailand Research Fund (TRF) and the Commission on Higher Education (CHE): Research Grant for New Scholar (MRG5280073), Ministry of Science and Technology, Thailand.

References

1. Jouini A, Gâcon JC, Ferid M, Trabelsi-Ayadi M. Luminescence and scintillation properties of praseodymium poly and diphosphates. Opt Mater. 2003;24:175–80.
2. Kitsugi T, Yamamuro T, Nakamura T, Oka M. Transmission electron microscopy observations at the interface of bone and four types of calcium phosphate ceramics with different calcium/phosphorus molar ratios. Biomaterials. 1995;16:1101–7.
3. Jian-Jiang B, Dong-Wan K, Kug Sun H. Microwave dielectric properties of $Ca_2P_2O_7$. J Eur Ceram Soc. 2003;23:2589–92.
4. Martinelli JR, Sene FF, Gomes L. Synthesis and properties of niobium barium phosphate glasses. J Non-Cryst Solids. 2000;263:299.
5. Carmen P, Josefina P, Regino SP, Caridad RV, Natalia S. Crystal growth, structure, and magnetic properties of a new polymorph of $Fe_2P_2O_7$. Chem Mater. 2003;15:3347–51.
6. Marcu I-C, Sandulescu I, Yves Schuurman Y, Millet J-MM. Mechanism of *n*-butane oxidative dehydrogenation over tetravalent pyrophosphates catalysts. Appl Catal A. 2008;334;207–16.
7. Boyle FW Jr, Lindsay WL. Diffraction patterns and solubility products of several divalent manganese phosphate. Soil Sci Soc Am J. 1985;49:761–6.
8. Boyle FW Jr, Lindsay WL. Manganese phosphate equilibrium relationships in soils. Soil Sci Soc Am J. 1986;50:588–93.
9. Bagieu-Beucher M. Structure cristalline du polyphosphate de manganèse trivalent $Mn(PO_3)_3$. Acta Crystallogr. 1978;B34:1443–6.
10. Lightfoot P, Cheetham AK, Sleight AW. Structure of manganese(3+) phosphate monohydrate by synchrotron X-ray powder diffraction. Inorg Chem. 1987;26:3544–7.
11. Nietubyć R, Sobzak E, Attenkofeer KE. X-ray absorption fine structure study of manganese compounds. J Alloys Compd. 2001;328:126–31.
12. Durif A, Averbuch-Pouchot MT. Structure du diphosphate acide de manganèse(III): $MnHP_2O_7$. Acta Crystallogr. 1982;B38:2883–5.
13. Massa W, Yakubovich OV, Dimitrova OV. A novel modification of manganese orthophosphate $Mn_3(PO_4)_2$. Solid State Sci. 2005;7:950–6.
14. Olbertz A, Stachel D, Svoboda I, Fuess H. Redetermination of the crystal structures of nickel cyclotetraphosphate, $Ni_2P_4O_{12}$ and of cobalt cyclotetraphosphate, $Co_2P_4O_{12}$. Z Kristallogr. 1995;210:241–2.
15. Stefanidis T, Nord AG. Structure studies of thortveitite-like dimanganese diphosphate, $Mn_2P_2O_7$. Acta Crystallogr. 1984;C40:1995–9.
16. El-Bali B, Boukhari A, Glaum R, Gerk M, Maaß K. Contributions on Crystal Structures and Thermal Behaviour of Anhydrous Phosphates. XXIX Preparation and Structure Determination of $SrMn_2(PO_4)_2$ and Redetermination of $SrMn_3(PO_4)_2$. Z Anorg Allg Chem. 2000;626:2557–62.

17. Schneider S, Collin RL. Crystal structure of manganese pyrophosphate dihydrate $Mn_2P_2O_7{\cdot}2H_2O$. Inorg Chem. 1973; 12:2136–9.
18. Aranda MAG, Attfield JP, Bruque S. Study of manganese phosphate or arsenate hydrates, $MnXO_4{\cdot}nH_2O$ (X = P, As), phases and synthesis and structure of the simple, novel salt $MnAsO_4$. Inorg Chem. 1993;32:1925–30.
19. Aranda MAG, Bruque S. Characterization of manganese(III) orthophosphate hydrate. Inorg Chem. 1990;29:1334–7.
20. Aranda MAG, Bruque S, Attfield JP. Crystal structures and characterization of a new manganese(III) arsenate, $MnAsO_4.1{\cdot}2H_2O$ and manganese(II) pyroarsenate, $Mn_2As_2O_7$. Inorg Chem. 1991;30:2043–7.
21. Stojakovic D, Rajic N, Sajic S, Logar NZ, Kaucic V. A kinetic study of the thermal degradation of 3-methylaminopropylamine inside $AlPO_4$-21. J Therm Anal Calorim. 2007;87:337–43.
22. Boonchom B, Youngme S, Srithanratana T, Danvirutai C. Synthesis of $AlPO_4$ and kinetics of thermal decomposition of $AlPO_4{\cdot}H_2O$-H_4 precursor. J Therm Anal Calorim. 2007;91:511–6.
23. Ozawa T. A new method of analyzing thermogravimetric data. Bull Chem Soc Jpn. 1965;38:1881–6.
24. Kissinger HE. Reaction Kinetics in Differential Thermal Analysis. J Anal Chem. 1957;29:1702–6.
25. Boonchom B, Youngme S, Maensiri S, Danvirutai C. Nanocrystalline serrabrancaite ($MnPO_4{\cdot}H_2O$) prepared by a simple precipitation route at low temperature. J Alloys Compd. 2006;454:78–82.
26. Witzke T, Wegner R, Doering T, PÖllmann H, Schuckmann W. Serrabrancaite, $MnPO_4{\cdot}H_2O$, a new mineral from the Alto Serra Branca pegmatite, Pedra Lavrada, Paraiba, Brazil. Amer Mineral. 2000;85:847–9.
27. Baril M, Assaaoudi H, Butler IS. Pressure-tuning Raman microspectroscopic study of cobalt(II), manganese(II), zinc(II) and magnesium(II) yrophosphate dihydrates. J Mol Struc. 2005; 751:168–71.
28. Harcharras M, Ennaciri A, Rulmont A, Gilbert B. Vibrational spectra and structures of double diphosphates $M_2CdP_2O_7$ (M = Li, Na, K, Rb, Cs). Spectrochim Acta. 1997;A53:345–52.
29. Brouzi K, Ennaciri A, Harcharras M, Capitelli F. Structure and vibrational spectra of a new trihydrate diphosphate, $MnNH_4NaP_2O_7{\cdot}3H_2O$. J Raman Spectrosc. 2004;35:41–6.
30. Vlaev LT, Nikolova MM, Gospodinov GG. Non-isothermal kinetics of dehydration of some selenite hexahydrates. J Solid State Chem. 2004;177:2663–9.
31. Vlase T, Vlase G, Brita N, Doca N. Comparative results of kinetic data obtained with different methods for complex decomposition steps. J Therm Anal Calorim. 2007;88:631–5.
32. Vlaev LT, Georgieva VG, Genieva SD. Products and kinetics of non-isothermal decomposition of vanadium(IV) oxide compounds. J Therm Anal Calorim. 2007;88:805–12.
33. Budrugeac P. The Kissinger law and the IKP method for evaluating the non-isothermal kinetic parameters. J Therm Anal Calorim. 2007;89:143–51.
34. Singh BK, Sharma RK, Garg BS. Kinetics and molecular modeling of biologically active glutathione complexes with lead(II) ions. J Therm Anal Calorim. 2006;84:593–600.
35. Vlaev L, Nedelchev N, Gyurova K, Zagorcheva M. A comparative study of non-isothermal kinetics of decomposition of calcium oxalate monohydrate. J Anal Pyrolysis. 2008;81:253–62.
36. Zhang K, Hong J, Cao G, Zhan D, Tao Y, Cong C. The kinetics of thermal dehydration of copper(II) acetate monohydrate in air. Thermochim Acta. 2005;437:145–9.
37. Boonchom B, Maensiri S, Danvirutai C. Soft solution synthesis, non-isothermal decomposition kinetics and characterization of manganese dihydrogen phosphate dihydrate $Mn(H_2PO_4)_2{\cdot}2H_2O$ and its thermal transformation products. Mater Chem Phys. 2008;109:404–10.
38. Boonchom B. Kinetics and thermodynamic properties of the thermal decomposition of manganese dihydrogenphosphate dihydrate. J Chem Eng Data. 2008;53:1553–8.
39. Boonchom B, Danvirutai C. A simple synthesis and thermal decomposition kinetics of $MnHPO_4{\cdot}3H_2O$ rod-like microparticles obtained by spontaneous precipitation route. J Optoelectron Adv Mater. 2008;10:492–9.
40. Boonchom B, Danvirutai C. Thermal decomposition kinetics of $FePO_4{\cdot}3H_2O$ precursor to synthetize spherical nanoparticles $FePO_4$. Ind Eng Chem Res. 2007;46:9071–6.
41. Boonchom B, Danvirutai C. Synthesis of $MnNiP_2O_7$ and nonisothermal decomposition kinetics of a new binary $Mn_{0.5}Ni_{0.5}HPO_4{\cdot}H_2O$ precursor obtained from a rapid coprecipitation at ambient temperature. Ind Eng Chem Res. 2008;47: 5976–81.
42. Noisong P, Danvirutai C, Srithanratana T, Boonchom B. Synthesis, characterization and non-isothermal decomposition kinetics of manganese hypophosphite monohydrate. Solid State Sci. 2008;10:1598–604.